Schweizerische Eidgenossenschaft
Confédération suisse
Confederazione Svizzera
Confederaziun svizra

Federal Department of the Environment, Transport, Energy and Communications DETEC

**Swiss Federal Office of Energy SFOE**
Energy Research and Cleantech

**Final report**

# SOLIFUEL

## Solar Dish-Reactor Technology for the Production of Liquid Transportation Fuels from $H_2O$ and $CO_2$

Source: ETH Zürich

ETH zürich

PREC
Professorship of Renewable Energy Carriers

**Date:** 13.12.2021

**Location:** Bern

**Publisher:**
Swiss Federal Office of Energy SFOE
Energy Research and Cleantech
CH-3003 Bern
www.bfe.admin.ch

**Subsidy recipients:**
ETH Zurich
Professorship of Renewable Energy Carriers
Sonneggstrasse 3 / ML J42.1
8092 Zürich
www.prec.ethz.ch

**Authors:**
Remo Schäppi, ETH Zurich, schremo@ethz.ch
Dr. Philipp Furler, ETH Zurich (presently at Synhelion)
Prof. Dr. Aldo Steinfeld, ETH Zurich, aldo.steinfeld@ethz.ch

**SFOE programme manager:** Dr. Stefan Oberholzer, stefan.oberholzer@bfe.admin.ch

**SFOE contract number:** SI/501213-01

# Zusammenfassung

Die gesamte Prozesskette zur Herstellung von flüssigen Treibstoffen aus konzentriertem Sonnenlicht und Umgebungsluft wurde erstmals in einer solaren Mini-Raffinerie unter realen Bedingungen auf dem Dach des ETH-Maschinenlaboratoriums demonstriert. Mit konzentriertem Sonnenlicht spaltet ein Hochtemperatur-Solarreaktor direkt aus der Luft extrahiertes $CO_2$ und $H_2O$ und produziert Syngas – ein spezifisches Gemisch aus $H_2$ und CO – das anschliessend zu flüssigen Kohlenwasserstoffen wie Methanol oder Kerosin verarbeitet wird. Der erfolgreiche Betrieb der solaren Demonstrationsanlage markiert einen wichtigen Meilenstein in der Herstellung von $CO_2$-neutralen synthetischen Treibstoffen, die bei der Verbrennung nur so viel $CO_2$ freisetzen wie vorher aus der Luft entnommen wurde. Diese Treibstoffe sind mit der weltweit bestehenden Infrastruktur für die Verteilung, Speicherung und Verwendung der Kraftstoffe kompatibel und können insbesondere zu einer nachhaltigen Luftfahrt beitragen.

# Summary

The entire thermochemical process chain to liquid hydrocarbon fuels from concentrated sunlight and ambient air was demonstrated for the first time in a solar mini-refinery system under real field conditions mounted on the roof of the ETH-Machine Laboratory. Using concentrated solar radiation, a high-temperature solar reactor splits $CO_2$ and $H_2O$ extracted directly from air and produces syngas – a specific mixture of $H_2$ and CO – which is finally processed into liquid hydrocarbons such as methanol or kerosene. The successful operation of the solar demonstration plant represents a crucial milestone towards the production of carbon-neutral synthetic fuels, which release only as much $CO_2$ during combustion as was previously extracted from the air. These are compatible with the worldwide existing infrastructures for fuel distribution, storage and utilization, and can particularly contribute to sustainable aviation.

# Main findings

Developing solar technologies for producing carbon-neutral transportation fuels has become a global energy challenge, especially for the long-haul aviation sector. A promising solution are drop-in fuels – synthetic alternatives for petroleum-derived liquid hydrocarbons such as kerosene, gasoline or diesel, which are compatible with the worldwide existing fuel infrastructures. Among the many possible approaches for solar-driven processes, the thermochemical path using concentrated solar radiation as the source of high-temperature process heat utilizes the entire solar spectrum and thus offers potentially high production rates and efficiencies. It can deliver truly carbon-neutral fuels if the required $CO_2$ is obtained directly from atmospheric air. If $H_2O$ is also co-extracted from air, feedstock sourcing and fuel production can be co-located in desert regions with high solar irradiation and limited access to water resources. While individual steps of such a scheme have been implemented, we now demonstrate the stable operation under real field conditions of the entire thermochemical solar fuel production chain to drop-in fuels from concentrated sunlight and ambient air. Crucial to this accomplished milestone is the serial integration of three thermochemical conversion processes, namely: 1) the co-extraction of $CO_2$ and $H_2O$ directly from air via an amine-based adsorption-desorption cycle; 2) the solar co-splitting of $CO_2$ and $H_2O$ to produce a tailored syngas mixture via a ceria-based redox cycle; and 3) the conversion of syngas to liquid hydrocarbons via Fischer-Tropsch or methanol synthesis. We further identify the R&D needs aimed at process optimization and upscaling towards the long-term decarbonisation of the aviation sector.

# Contents

**Zusammenfassung** ..... **3**

**Summary** ..... **3**

**Main findings** ..... **3**

**Contents** ..... **4**

**1 Introduction** ..... **5**

1.1 Background information and current situation ..... 5

1.2 Objectives ..... 5

**2 Description of facility** ..... **6**

2.1 The Direct Air Capture Unit ..... 6

2.2 The Solar Redox Unit ..... 7

2.3 The Gas-to-Liquid Unit ..... 11

**3 Procedures and methodology** ..... **12**

**4 Results and discussion** ..... **12**

4.1 Solar flux measurements ..... 12

4.2 Solar redox cycles ..... 13

4.3 Solar syngas suitable for methanol or Fischer-Tropsch synthesis ..... 15

4.4 Mass balance ..... 16

4.5 Long-term consecutive solar redox cycling for methanol production ..... 17

4.6 Integration of the solar fuel system ..... 18

4.7 Efficiency ..... 18

**5 Conclusions** ..... **21**

**6 Outlook and next steps** ..... **21**

**7 National and international cooperation** ..... **22**

**8 Communication** ..... **23**

**9 Publications** ..... **24**

9.1 Papers in refereed journals ..... 24

9.2 Conference contributions ..... 24

9.3 Invited talks ..... 26

**10 References** ..... **27**

# 1 Introduction

## 1.1 Background information and current situation

The aviation and shipping sectors are strongly dependent on liquid hydrocarbon fuels derived from fossil fuels and are contributing approximately 6% of the total anthropogenic $CO_2$ emissions[1,2]. Based on projected growth, this proportion could progressively become a dominant $CO_2$-emissions source[2,3], but the decarbonization of these transportation sectors via battery-driven electric propulsion is unfeasible for long haul commercial travel[4]. Alternatively, drop-in fuels – synthetic and completely interchangeable substitutes for conventional petroleum-derived hydrocarbons (e.g. kerosene, gasoline, diesel, methanol) – can be synthesized from $H_2O$ and $CO_2$ using solar energy[5,6]. Various solar-driven paths have been proposed based on electrochemical, photochemical, and thermochemical processes and their combinations[7]. In particular, the thermochemical path using concentrated solar radiation as the source of process heat inherently operates at high temperatures and utilizes the entire solar spectrum, and as such provides a favorable thermodynamic path with potentially high rates and efficiencies[8]. However, in contrast to biofuels that naturally close the anthropogenic carbon fuel cycle, the solar-driven approach should include the extraction of $CO_2$ directly from atmospheric air – the so-called direct air capture (DAC) process – to produce truly carbon-neutral hydrocarbon fuels for the transportation sectors[9]. If, additionally, $H_2O$ is co-extracted from air[10], logistical benefits can be gained, as the DAC plant can then be strategically located next to the solar fuel plant in desert regions with high direct normal solar irradiation (DNI) but limited access to water resources.

Yet, most studies to date on the production of solar fuels from $H_2O$ and $CO_2$ using DAC have largely been limited to bench-top[11,12] or pilot-scale[13,14] demonstrations of individual steps as low specific fuel yields or poor materials stability have prevented to integrate all steps of the fuel production chain and/or to advance the technology readiness level beyond the laboratory stage. One pertinent experimental proof-of-concept that integrated all steps was the PV-electrolysis based system[15], but it also used fossil derived syngas for the hydrocarbon synthesis because of the challenge of coupling intermittent solar with continuous non-solar processes requiring the delivery of chemicals at specific rates and purity.

## 1.2 Objectives

This project is aimed at the design, fabrication, and experimental demonstration of the complete modular solar dish-reactor system for producing solar liquid fuels from $H_2O$ and $CO_2$ captured from air. The system encompasses a novel high-flux solar parabolic concentrator coupled to a solar thermochemical reactor, a gas-to-liquid processing unit and a $CO_2/H_2O$ air capture unit. The solar reactor subsystem consists of two side-by-side cavity-receivers containing dual-scale reticulated porous ceramic (RPC) for producing syngas via ceria-based redox cycling. The experimental validation of the complete process chain to solar liquid hydrocarbon fuels at a pre-commercial scale, by moving from a laboratory setup to a modular solar system, will advance the technological readiness and its industrial implementation.

# 2 Description of facility

The solar fuel system, realized on the roof of the ETH's Machine Laboratory Building in Zurich, is shown schematically in Figure 1. It serially integrates three thermochemical conversion units, namely:

1) the direct air capture (DAC) unit which co-extracts $CO_2$ and $H_2O$ directly from ambient air;
2) the solar redox unit which converts $CO_2$ and $H_2O$ into a desired mixture of CO and $H_2$ (syngas); and
3) the gas-to-liquid (GTL) unit which converts syngas to liquid hydrocarbons or methanol.

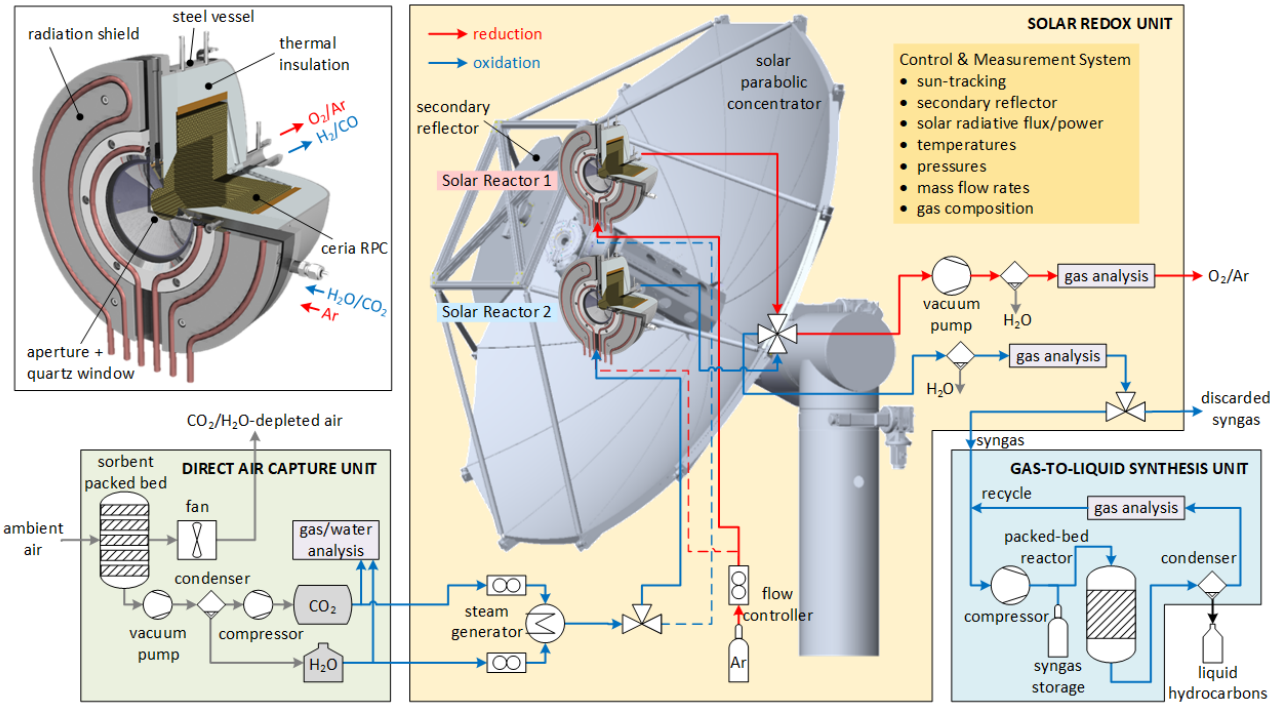


**Figure 1.** Simplified process chain of the solar fuel system integrating three thermochemical conversion units in series: 1) the direct air capture (DAC) unit which co-extracts $CO_2$ and $H_2O$ directly from ambient air; 2) the solar redox unit which converts $CO_2$ and $H_2O$ into a desired mixture of CO and $H_2$ (syngas) using concentrated solar energy; and 3) the gas-to-liquid (GTL) synthesis unit which finally converts syngas to methanol or liquid hydrocarbons. Two identical solar reactors are positioned at the focus of the solar concentrator for performing both redox steps of the thermochemical cycle simultaneously by alternating the concentrated solar input between them. While one solar reactor is performing the endothermic reduction step on sun, the second solar reactor is performing the exothermic oxidation step off sun. Red arrow indicates reduction (Eq. 1); blue arrow indicates oxidation (Eq. 2a/2b). Dimensions are not to scale. *Upper-left insert*: Cross-section of the solar reactor featuring a cavity-receiver containing a reticulated porous ceramic structure (RPC) made of pure ceria for performing the thermochemical redox cycle.

## 2.1 The Direct Air Capture Unit

The DAC unit, being commercialized by the ETH's spinoff Climeworks, is based on an adsorption-desorption cyclic process. Temperature-vacuum swing is applied to an amine-functionalized sorbent to concurrently extract $CO_2$ and $H_2O$ from ambient air[10]. Adsorption proceeds at ambient temperature and pressure for 180 minutes per cycle while desorption proceeds at 95°C and 0.1-0.3 bar for 43 minutes per cycle. This unit can process an air flow of 2000 $m^3$/hr with 5.5 cycles/day, yielding around

8 kg/day of $CO_2$ with a measured purity of 98% (the remainder being air), along with 20-40 kg/day of pure water (depending on air relative humidity) with contaminants below the 0.2 ppm detection limit. The exhaust air has a $CO_2$ depletion extent in the range 40-70%. The $CO_2$ stream exiting the DAC unit during desorption is collected in a balloon-type buffer reservoir at ambient pressure, subsequently compressed to maximum 12 bars, and intermediately stored in a 750 l steel buffer tank. Water is condensed out of the desorption stream and intermediately stored in a plastic buffer tank. With this arrangement, both $CO_2$ and $H_2O$ are delivered from their buffer tanks to the solar redox unit on demand. The calculated specific energy requirements are 13 kJ/mol$_{CO2}$ of mechanical work (vacuum pump operated at 0.05 bar desorption pressure/1 bar exit pressure and with 0.7 efficiency of isothermal compression), and 493-640 kJ/mol$_{CO2}$ of heat at 95°C for an air relative humidity in the range 20-80%. For a targeted sorbent's specific $CO_2$ capacity of 2 mmol/g, the heat requirement would be reduced to 272 kJ/mol$_{CO2}$. Obviously, higher relative humidity results in more water adsorbed and, consequently, higher thermal energy requirements during the desorption step.

### 2.2 The Solar Redox Unit

The solar redox unit is based on the thermochemical splitting of $CO_2$ and $H_2O$ via a reduction-oxidation (redox) cycle driven by concentrated solar process heat[8]. Nonstoichiometroic ceria ($CeO_{2-\delta}$) is selected as the redox material because of its rapid kinetics, crystallographic stability, and abundance in the earth's crust comparable to that of copper[16,17]. Alternative redox materials, e.g. perovskites[18-20], have been assessed for superior redox performance, but have not yet proven to be as reliable as ceria. The redox cycle with ceria, represented by the reactions listed in Table 1, comprises two steps. In the first endothermic step, ceria is thermally reduced to generate $O_2$ (eq. 1). In the second exothermic step, the reduced ceria is re-oxidized with $CO_2$ and/or $H_2O$ to generate CO and/or $H_2$ (eqs. 2a and 2b), respectively. Thus, ceria is not consumed and the net reactions are: $CO_2$=CO+½$O_2$ and $H_2O$=$H_2$+½$O_2$, but the fuel ($H_2$, CO) and $O_2$ are generated in different steps, thereby avoiding an explosive mixture and eliminating the need for high-temperature gas separation. We apply both temperature and pressure swing to maximize the oxygen exchange capacity of ceria, and thereby the fuel yield per cycle[21-25]. $\delta$ denotes the non-stoichiometry – the measure of the redox extent which, in equilibrium, is a function of temperature and oxygen partial pressure. For typical operating conditions of the reduction step at 1450°C and 0.1 mbar and the oxidation step at 900°C and 1 bar, thermodynamic predicts $\Delta\delta = \delta_{red}-\delta_{ox} = 0.04$.

**Table 1.** Redox reactions and the corresponding enthalpy change of the 2-step thermochemical cycle for splitting $CO_2$ and $H_2O$ using nonstoichiometric ceria.

| | | |
|---|---|---|
| Reduction: $\Delta H \approx 475$ kJ per ½ mole $O_2$ | $\frac{1}{\Delta\delta}\mathrm{CeO}_{2-\delta_{ox}} \rightarrow \frac{1}{\Delta\delta}\mathrm{CeO}_{2-\delta_{red}} + \frac{1}{2}\mathrm{O}_2$ | (1) |
| Oxidation with $CO_2$: $\Delta H \approx$ -192 kJ/mol $CO_2$ | $\frac{1}{\Delta\delta}\mathrm{CeO}_{2-\delta_{red}} + \mathrm{CO}_2 \rightarrow \frac{1}{\Delta\delta}\mathrm{CeO}_{2-\delta_{ox}} + \mathrm{CO}$ | (2a) |
| Oxidation with $H_2O$: $\Delta H \approx$ - 234 kJ/mol $H_2$ | $\frac{1}{\Delta\delta}\mathrm{CeO}_{2-\delta_{red}} + \mathrm{H}_2\mathrm{O} \rightarrow \frac{1}{\Delta\delta}\mathrm{CeO}_{2-\delta_{ox}} + \mathrm{H}_2$ | (2b) |

*The solar reactor* − The solar reactor development evolved from its early design[26] to its present configuration[27] with the help of CFD simulations[28] and superior redox material structures[29]. Its configuration is shown schematically in Figure 1 (insert). It consists of a cavity-receiver with a circular aperture sealed by a quartz window for the access of concentrated solar radiation. The cavity contains a reticulated porous ceramic (RPC) structure made of ceria with dual-scale interconnected porosity in

the mm and µm ranges for enhanced heat and mass transfer[29]. The main components of the solar reactor are schematically shown in Figure 2. The ceria RPC is contained within the cavity and consists of 8 bricks and 1 octagonal back plate to form an octagonal cavity with 120 mm-i.d., 190 mm-o.d. and 110 mm in height. The octagonal assembly was chosen to allow thermal and chemical expansion of the RPC parts without inducing extensive stress. Figure 3 a) and b) show photographs of the RPC reactor parts and the RPC's mounted in the solar reactor, respectively.

Since only the endothermic reduction step requires a solar input, two identical solar reactors are employed for performing both redox steps simultaneously by alternating the concentrated solar input between them. The optical configuration of the solar concentrator that enables this alternation of the focus consists of a primary sun-tracking paraboloidal concentrator coupled to a secondary planar rotating reflector[30]. For a DNI = 1 kW/m$^2$, it alternately delivers a solar radiative power up to 7.7 kW at a peak flux concentration of 5,010 suns and an average flux of 2,710 suns measured over the 30 mm-radius aperture of each solar reactor.

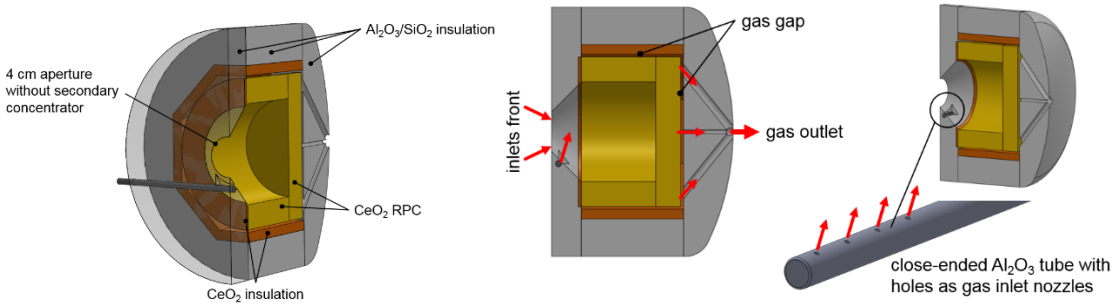


**Figure 2.** Configuration of the solar reactor design

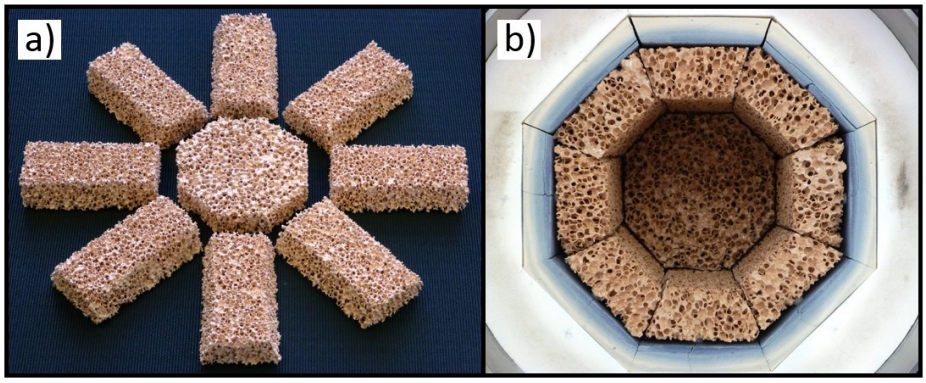


**Figure 3.** a) RPC parts for solar reactor consisting of 8 brick elements and 1 octagonal backplate; b):RPC mounted in octagonal shape inside cavity receiver.

*Solar concentrator* – Figure 4a) shows a 3D rendering and photograph of the final solar dish system, comprising the two-axis sun-tracking primary parabolic dish, the rotating secondary flat reflector with its mounting structure and motor. Fig. 4b) depicts a close-up on the instrumentation mounted at the focal plane: the two solar reactors, a white Lambertian target for the optical flux measurements, and a water-cooled calorimeter. A side view on the system with its main geometrical parameters is shown in Fig. The primary parabolic dish consists of 12 individual panels yielding a dodecagonal shape with focal length $f = 2.2$ m, outer radius in the range $2.19\ \text{m} \le R_o \le 2.24$ m, rim angle in the range $52.7° \le \phi \le 53.9°$, and projected total and illuminated area of 15.3 m$^2$ and 12.9 m$^2$, respectively. For

the 30 mm aperture of the solar reactors, the full system achieves a geometric concentration ratio of $C_{geo} = A_{dish}/A_{reactor}$ = 4,560. For both primary and secondary reflectors, 160 × 160 × 1 mm highly reflective back-silvered float-glass reflectors (Fast Glass, 2017) were glued onto the support structure.

The secondary planar reflector has an area $A_2$ = 1.71 m$^2$ and tilt angle $\beta/2$ = 12°. It was designed and positioned such that all rays coming from the primary reflector are intercepted and directed to the focal point which is displaced by $R_f$ = 0.2 m from the primary optical axis. The outline of the planar secondary is given by the intersection of a tilted flat plane and a cone with the dish's rim as the base and the apex slightly above the primary focal point. The apex is positioned such that radiation deviating up to 0.5° (8.73 mrad) away from the focal point is still intercepted, accounting for the solar angular subtense of 4.65 mrad as well as for tracking errors and primary shape inaccuracies. The tilt of the secondary reflector $\beta/2$, where $\beta$ is the angle between the primary and secondary optical axes, is determined by the distance $R_f$ by which the focus needs to be displaced and its distance to the focal point. A larger tilt places the secondary closer to the focal point, while a lower tilt moves it further away. $\beta$ was chosen to minimize losses caused by shading and blocking in the system. The yellow dotted lines in Fig. 5 indicate the three regions prone to shading and blocking: (1) shading of the primary reflector by the secondary reflector, (2) blocking between primary and secondary reflectors by instruments, and (3) blocking between secondary reflector and focus by instruments. For configurations with no collisions between secondary reflector and instruments, the size of the secondary reflector decreases with increasing tilt angle, therefore leading to lower losses by shading but at the expense of higher losses by blocking. The optimum was found for $\beta$ = 24°, which results in a relatively large secondary reflector with 11.1% shading losses and 1.7% blocking losses.

All instruments are mounted on a common instrument holder fixed axially at the center of the primary parabolic dish concentrator. The solar reactors, the water calorimeter, and the Lambertian target are tilted by $\beta$ = 24° and with their aperture's centers positioned along the circular focal point trajectory as the secondary rotates (see red dashed circle in Fig. 4b). An accurate focal position is guaranteed by two-axis tracking (azimuth/altitude) using two three phase AC motors (Lenze IE1 MD071) which follows a pre-calculated path (Reda and Andreas, 2004). The dish's orientation is then fine-tuned using a solar sensor (Solar MEMS ISS-D5, precision = 0.005°). The secondary reflector is rotated using a slotless, brushless rotary motor (Aerotech BMS60).

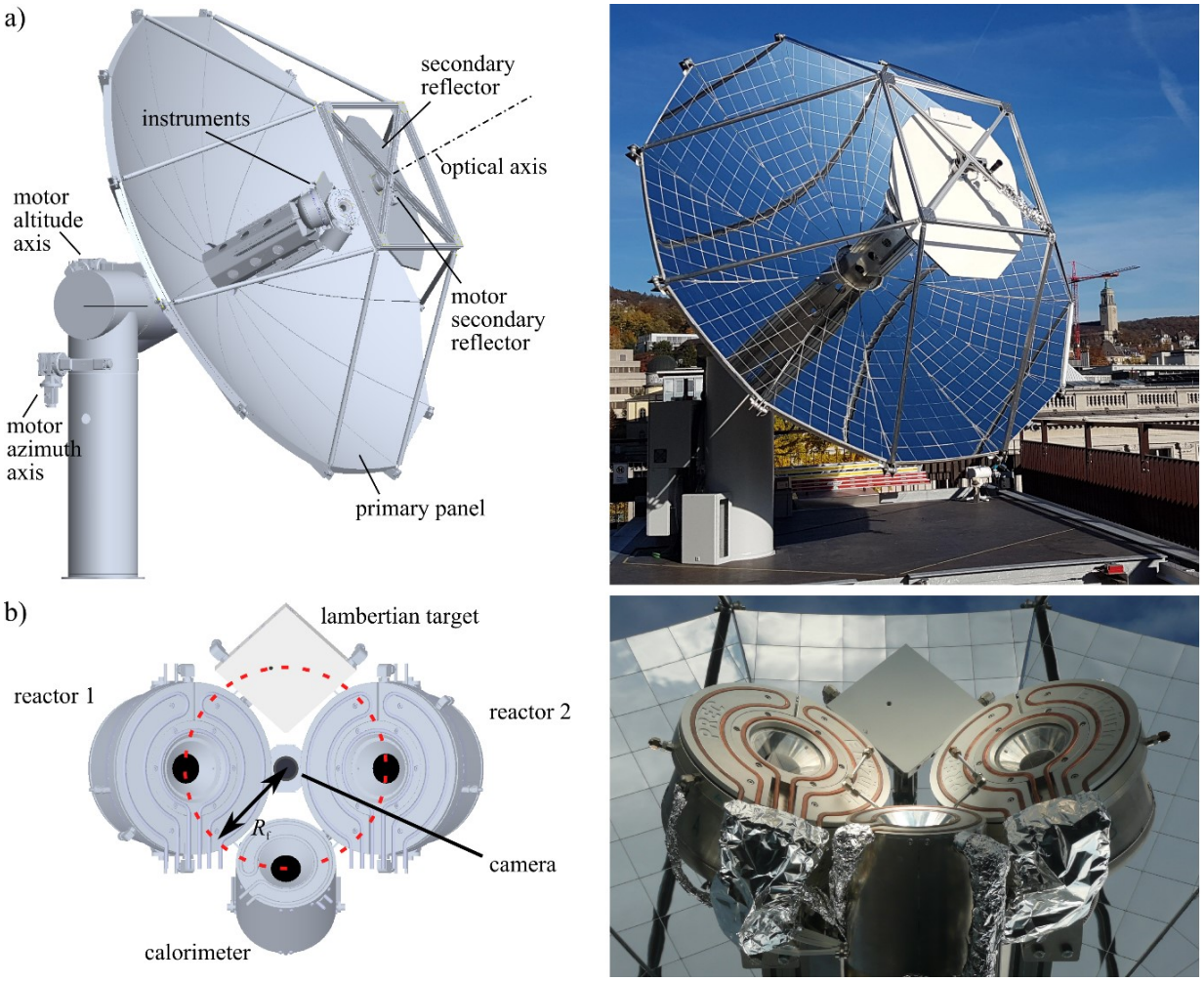


**Figure. 4.** Schematics and photographs of the solar dish system: a) 3D rendering of the primary two-axis sun-tracking parabolic dish and secondary rotating flat reflector; b) solar reactors, water-cooled calorimeter, and Lambertian target. The dashed circle indicates the focal point trajectory during rotation of the secondary reflector.

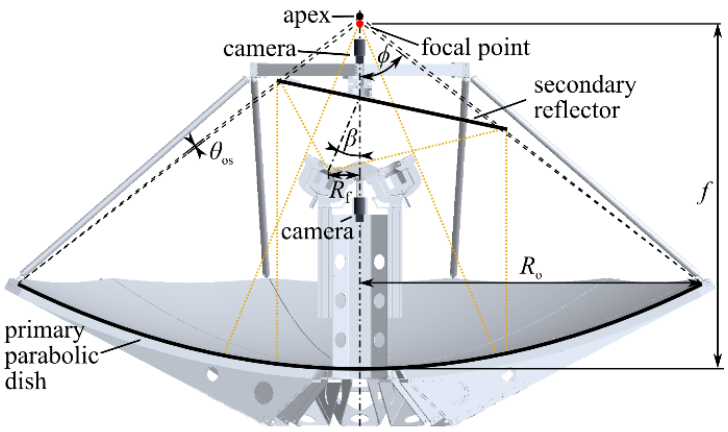


**Figure 5.** Side view of solar dish system depicting the major optical quantities: $f$ = 2.2 m, 2.185 m ≤ $R_o$ ≤ 2.244 m, $R_f$ = 0.2 m, 52.65° ≤ $\phi$ ≤ 53.92°, $\beta$ = 24°, $\vartheta_{os}$ = 0.5° ≈ 8.73 mrad.

*Housing and infrastructure* – The solar dish-reactor system was mounted on the roof of the Maschinenlaboratorium ML-Building at ETH Zurich. The system is protected by a steel housing from weather conditions (e.g. strong winds, rain, and snow) when not in operation. The housing is mounted on rails and can be horizontally moved by an electric cable winch to uncover the solar dish-reactor system. Figure 6 shows the side and top views of the housing: (1) in park position when the system is not in operation and (2) when moved during operation.

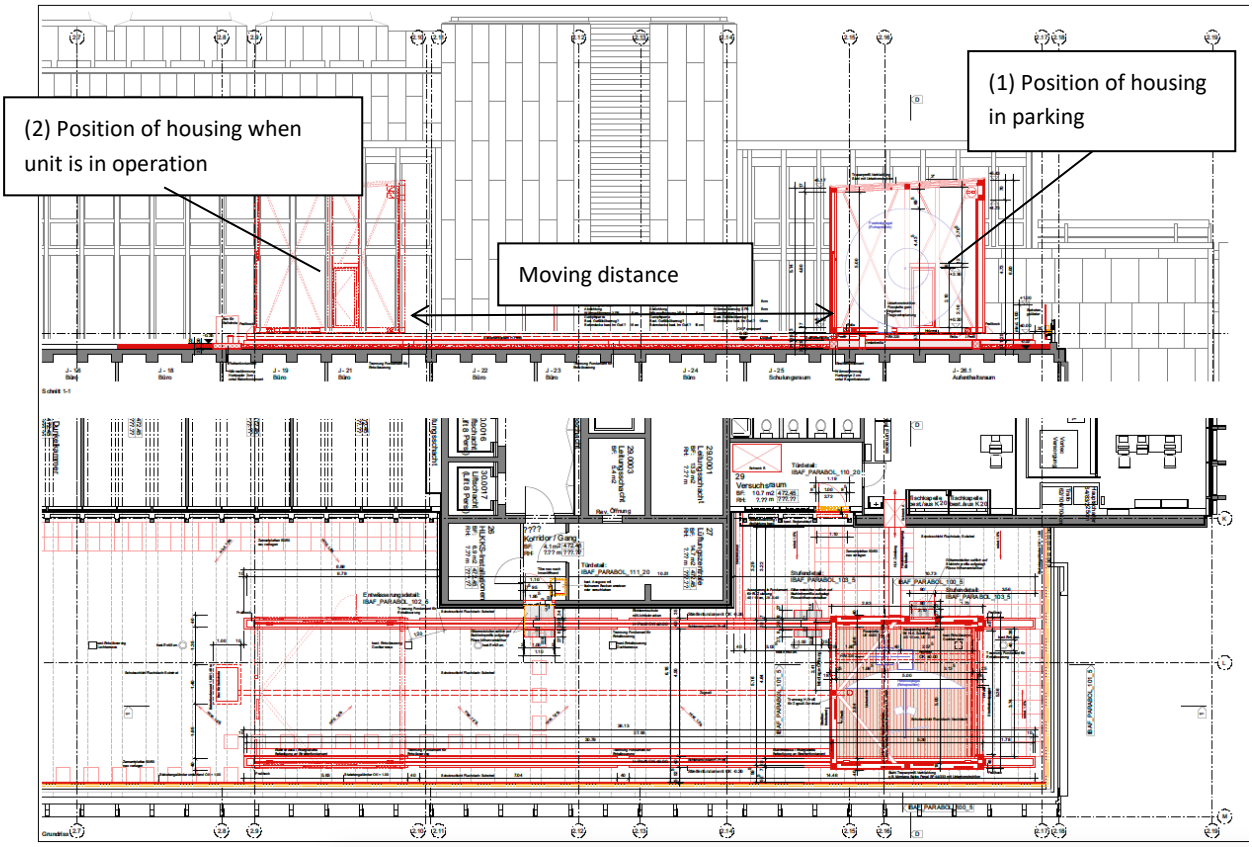


**Figure 6:** Top and side views of the housing on the roof of the Maschinenlaboratorium ML-Building at ETH Zurich.

## 2.3 The Gas-to-Liquid Unit

Downstream of the solar redox unit (Fig. 1), the $O_2$ stream evolving from the reduction step is analyzed and vented. The syngas stream evolving from the oxidation step is analyzed and sent to the GTL unit, where it is first compressed and intermediately stored in a 5-liter buffer gas cylinder at up to 250 bar. Finally, solar syngas is processed to methanol using a commercial Cu-ZnO-$Al_2O_3$ catalyst (Product No. 45776, Alfa Aesar) in a packed-bed tubular reactor at 230 °C and 50 bars. This final process step is mature and does not include technological innovations. The single-pass molar conversion of the GTL unit was 27%, yielding methanol with a purity of 65%, the rest being pure water (contaminants below the detection limit, e.g. ethanol and butanol < 1 ppm, propanol < 10 ppm). The remaining unconverted syngas was recycled for multiple passes through the GTL unit. However, since Ar concentration increased with each pass, the recycled syngas was discarded after 6 consecutive passes.

# 3 Procedures and methodology

Temperatures were measured using B-type and K-type thermocouples. Gas flow rates were regulated using Bronkhorst electronic mass flow controllers. Pressures were measured using THERMOVAC TTR 101N pressure sensors. A multistage roots dry vacuum pump (Adixen ACP 28CV) in combination with multiple valves (Pfeiffer Vacuum AVC 025 PA) was used to evacuate the reactors during reduction. Product gas composition was analyzed on-line downstream of the solar redox unit by gas chromatography (Agilent Technologies) and Siemens Ultramat 23 and Calomat 6 gas analysis units (electrochemical sensors for $O_2$, IR detectors for CO and $CO_2$, thermal conductivity based detectors for $H_2$). The syngas was compressed using the two stage Compressor Station ILS 331. The packed-bed reactor GTL synthesis unit was a Microactivity Effi (PID Eng&Tech). The direct normal irradiation (DNI) was measured with a sun-tracking pyrheliometer (EKO Instruments MS-56). The solar radiative power delivered by the solar concentrating system was measured using a water-cooled calorimeter made of a selectively coated Cu-coiled cavity with the same front containing the 30 mm-radius aperture as the solar reactors. The solar flux distribution was measured with a calibrated CCD camera (Basler scA1400-17gm, manual zoom lens RICOH FL-CC6Z1218-VG, neutral density filters ND 4.8) focused on a Lambertian (diffusely-reflecting) target and verified with the water-cooled calorimeter. Both the Lambertian target and the water-cooled calorimeter were mounted at the focal plane alongside the two solar reactors. The entire solar redox unit is controlled by a LabView program for performing fully automated consecutive redox cycles over the whole day.

# 4 Results and discussion

## 4.1 Solar flux measurements

Measurements were performed for two cases: (a) the stand-alone primary dish concentrator; and (b) the complete system including secondary reflector. Fig. 7 shows the measured solar concentration ratio distribution on the Lambertian target for both cases. For case (a), $C_{peak}$ = 10,160 suns peak and $C_{mean}$ = 3,630 suns over a 30 mm-radius circular area. For case (b): $C_{peak}$ = 5,010 suns peak and $C_{mean}$ = 2,660 suns over a 30 mm-radius circular area. Integration of $C$ over that area and normalized to $E_{bn}$ = 1 kW m$^{-2}$ yields $\dot{Q}$ =10,260 W and 7,520 W for the cases (a) and (b), respectively. The corresponding intercept factor is $\gamma$ = 78.8 and 70.3%, respectively. The main reasons for the decrease in performance for case (b) are: 1) the introduction of the additional reflection ($\rho_2$ = 94.3%) as well as angular scattering due to reflector slope errors resulting in a lower intercept factor; and 2) the inlet aperture of the primary reflector is reduced from 15.0 m$^2$ to 12.9 m$^2$ due to shading by the secondary reflector and its support structure. Since the shading occurs in the center of the parabolic dish, which is most tolerant to slope errors, it also negatively affects the intercept factor.

To collect a part of the spillage around the 30 mm-radius aperture, a reflective frustum is implemented in front of the focal plane (see Fig. 4b), increasing the intercept factor to $\gamma$ = 71.4%. For the 30 mm-radius aperture, $\dot{Q}_{reactor}$ = 7,680 W with $C_{mean}$ = 2,710 suns and $C_{peak}$ = 5,010 suns. The validity of the optical measurements is confirmed by comparison with the water calorimeter measurements. The relative difference between the two independent methods is 0.7%.

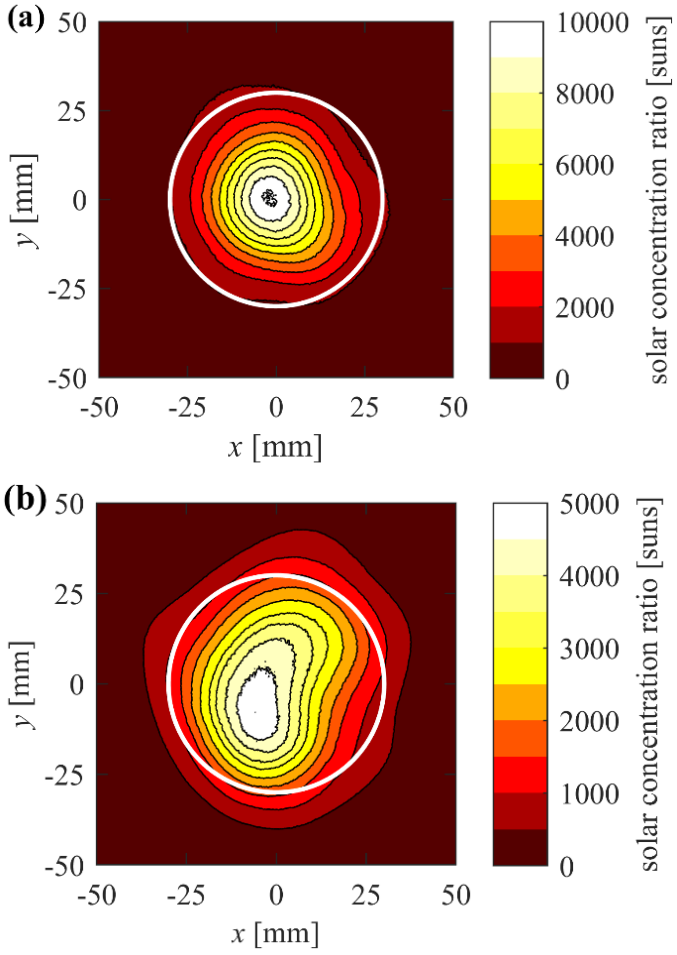


**Figure 7.** Solar concentration ratio distribution measured for: a) the stand-alone primary dish concentrator; and b) the complete system including secondary reflector. The white circle indicates the 30-mm-radius circular area, which corresponds to the size of the solar reactor's aperture.

### 4.2 Solar redox cycles

The solar redox unit enables the splitting of pure $CO_2$, pure $H_2O$, and both $H_2O$ and $CO_2$ simultaneously. Figure 8 shows a representative 7-hour day run with 17 consecutive redox cycles for co-splitting $H_2O$ and $CO_2$, yielding 96.2 L (standard liters) of syngas with composition 59.5% $H_2$, 4.6% CO, 17.5% $CO_2$, and 18.4% Ar. The oxygen mass balance confirmed total selectivity for the conversion of $H_2O$ to $H_2$ and of $CO_2$ to CO. The daily mass specific yield of syngas was 12.81 L/kg of ceria and its cumulative molar ratio $H_2$:$CO_x$ was 2.7. As the DNI varied with time, the inlet gas flows were adjusted to match the duration of the reduction step with that of the oxidation step, enabling the switching of the solar input between the two solar reactors without delay and, thus, making continuous use of the solar input. In this specific day run, the targeted syngas quality was the one suitable for methanol synthesis.

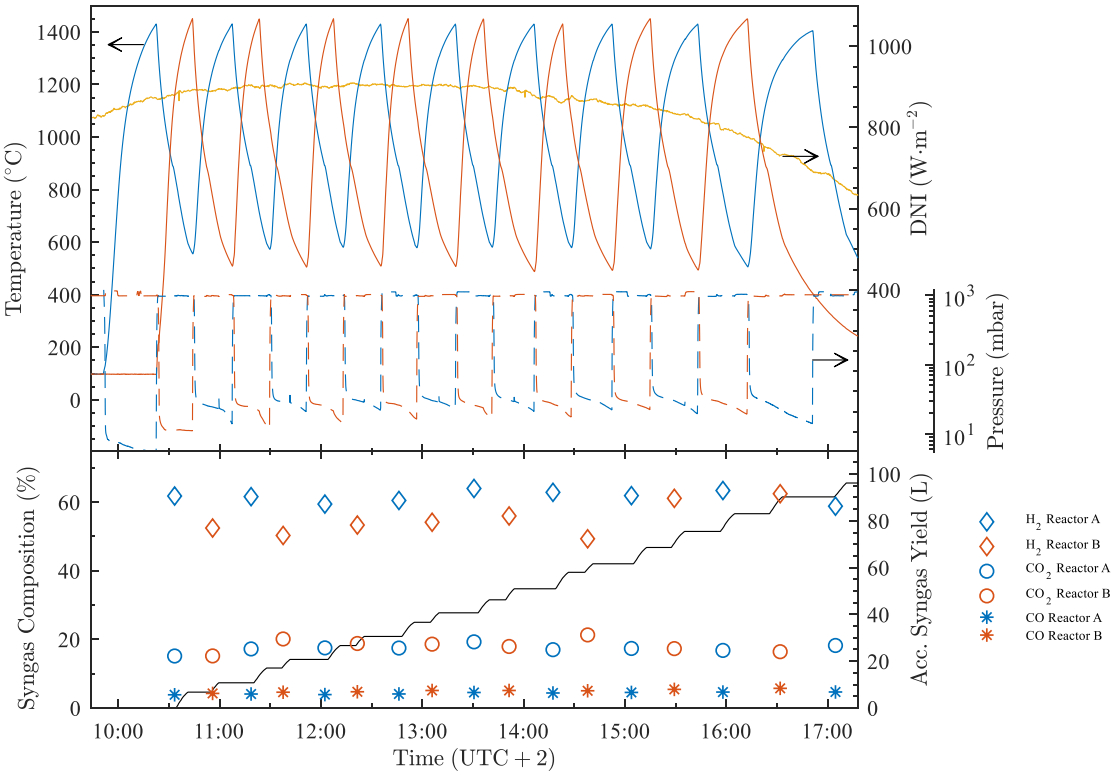


**Figure 8.** Representative day run of the solar redox unit for co-splitting $H_2O$ and $CO_2$. Temporal variations of the direct normal solar irradiation (DNI), temperature, pressure, syngas composition, and cumulative syngas yield of the two adjacent solar reactors A and B (blue and red curves, respectively) performing the thermochemical redox cycle simultaneously. The concentrated solar radiative input is alternated between the solar reactors A and B: while one reactor is solar irradiated to effect the reduction step (eq. S1), $H_2O$ and $CO_2$ are injected in the second reactor to effect the oxidation step (eqs. 2a and 2b). Inlet mass flow rates: 0.5 L/min Ar during reduction; 0.3 L/min $CO_2$ and 9.8 g/min $H_2O$ during oxidation. L denotes standard liters.

Depending on the catalyst used in the GTL unit, the desired $H_2$:$CO_x$ molar ratio of syngas for methanol synthesis lies between 2 and 3, while the desired $H_2$:CO molar ratio of syngas for FT-synthesis is about 2. The syngas composition, especially the molar ratios $H_2$:CO and CO:$CO_2$, can be controlled by adjusting the $H_2O$:$CO_2$ feed ratio to the solar reactor[31] and/or by performing separately the splitting of $CO_2$ and $H_2O$[26,27,32] and/or by simply choosing appropriate start and end times of the syngas collection. In either case, the syngas purity and quality is suitable for GTL processing and can be tailored for methanol or FT synthesis, respectively, without the need of additional steps for correcting composition and/or separating undesired by-products. Especially, the need for the endothermic reverse water-gas shift (RWGS) step is eliminated. In this study, the GTL unit was applied for processing solar syngas to methanol. FT synthesis of kerosene was performed with solar syngas obtained in two separate experimental setups using the same solar reactor design: with a 4-kW solar reactor prototype operated in a high-flux solar simulator[33] and with a scaled-up 50-kW solar reactor operated in a solar tower[34,35]. Obviously, there is no need for removal of any impurities (e.g. sulfur compounds, salts, heavy metals), as it is the case for hydrocarbons derived from petroleum. Moreover, the combustion of FT-based jet fuel, which is aromatic- and sulfur-free and is certified as aviation turbine fuel after the standard specification ASTM7566, showed dramatic reductions in soot emissions compared to fossil-based jet fuel[36].

### 4.3 Solar syngas suitable for methanol or Fischer-Tropsch synthesis

Figures 9 and 10 show two cases of an exemplary redox cycle for co-splitting $H_2O$ and $CO_2$ and producing solar syngas with compositions suitable for either methanol synthesis (Fig. 9) or FT synthesis (Fig. 10). The temporal variation of the nominal cavity temperature, total pressure, and outlet gas flow rates during a single redox cycle are plotted for both cases in Figs. 9a and 10a. The solar radiative power input is maintained relatively constant on a clear sunny day at $Q_{solar}$ = 5.1 kW (run of Fig. 9a) and 4.1 kW (run of Fig. 10a). In both cases, the reduction step proceeds under analogous operational conditions: the solar reactor is first heated with $Q_{solar}$ to the desired reduction-end temperature $T_{reduction\text{-}end}$ = 1450°C under vacuum pressure below 50 mbar. Once a nominal cavity temperature of $T_{reduction\text{-}end}$ is reached, the solar input is diverted by rotating the secondary reflector. Subsequently, the reaction chamber is re-pressurized to 1 bar by injecting either Ar for the case of syngas for methanol synthesis (Fig. 9a) or $CO_2$ for the case of syngas for FT synthesis (Fig. 10a). Passive cooling of the solar reactor induces a temperature decrease down to the oxidation-start temperature, $T_{oxidation\text{-}start}$ = 900°C and 850°C for the two cases, respectively. At that point, $H_2O$ and $CO_2$ from the buffer tanks are co-injected into the solar reactor with molar ratios $H_2O$:$CO_2$ = 12.5 and 24.9, to produce desired compositions of syngas for either methanol (Fig. 9) or FT synthesis (Fig. 10), respectively. The temporal variation of the cumulative species concentrations and yields of solar syngas collected during the oxidation step for either methanol or FT synthesis are plotted in Fig. 9b and Fig. 10b, respectively. Time 0 denotes the start of the oxidation when the nominal reactor temperature reaches $T_{oxidation\text{-}start}$. Note the absence of Ar in the syngas for FT synthesis because $CO_2$ was used instead to re-pressurize the solar reactor after the reduction step. Apart from selecting the $T_{oxidation\text{-}start}$ and the inlet flow rates of $H_2O$ and $CO_2$, the composition of the syngas can be adjusted by choosing adequate start and end times of the syngas collection. For example, immediately after the start of the oxidation step, the syngas contains undesired high Ar (Fig. 9b) or $CO_2$ content (Fig 10b), but we can improve the syngas quality by simply delaying the start of the syngas collection. On the other hand, the end of the syngas collection can be determined once the desired molar ratio $H_2$:$CO_x$ or $H_2$:CO of the collected syngas is achieved. In fact, the desired molar ratio $H_2$:$CO_x$ of syngas suitable for methanol synthesis lies between 2 and 3, depending on the CO:$CO_2$ molar ratio and on the catalyst used.

In the analysis that follows, we show how the yield and composition of the solar syngas can be adjusted by simply choosing adequate start and end times of the syngas collection. For the case of syngas for methanol synthesis (Fig. 9b), the full oxidation after 20 min yields 18.5 L* of syngas with composition 40.7% $H_2$, 4.3% CO, 22.4% $CO_2$ and 32.6% Ar. The resulting molar ratio $H_2$:$CO_x$ is 1.52, which is not optimal for methanol synthesis. Besides, the $CO_2$ conversion – integrated over the full oxidation period – is only 16.1%. Alternatively, collecting the syngas between minutes 2 and 10 (Fig. 9b) would yield instead only 9.4 L of syngas, i.e. only about half the amount, but with a more favorable composition of 59.9% $H_2$, 6.0% CO, 17.2% $CO_2$ and 16.9% Ar. The resulting molar ratio $H_2$:$CO_x$ would be 2.58, and thus suitable for methanol synthesis. The $CO_2$ conversion – integrated over minutes 2 to 10 – would be now 25.7%. Furthermore, the Ar content would be cut in half, reducing the energy penalty of carrying an inert gas downstream.

For the case of syngas for FT synthesis (Fig. 10b), the full oxidation after 25 min yields 15.6 L of syngas with composition 31.0% $H_2$, 11.4% CO and 57.6% $CO_2$ with a molar ratio $H_2$:CO = 2.72, which is not optimal for FT synthesis. The $CO_2$ conversion – integrated over the full oxidation period – is only 16.5%. Alternatively, collecting the syngas between minutes 0 and 4.25 (Fig. 10b) would yield only 7.52 L of syngas, i.e. only about half the amount, but with a more favorable composition of 43.1% $H_2$, 21.5% CO

* L denotes liters at standard conditions (0°C and 1 bar).

and 35.4% $CO_2$. The resulting molar ratio would be exactly $H_2$:CO = 2, and thus suitable for FT synthesis. The $CO_2$ conversion – integrated over minutes 0 to 4.25 – would now be 37.9%. Evidently, there is a trade-off between syngas quality and syngas quantity.

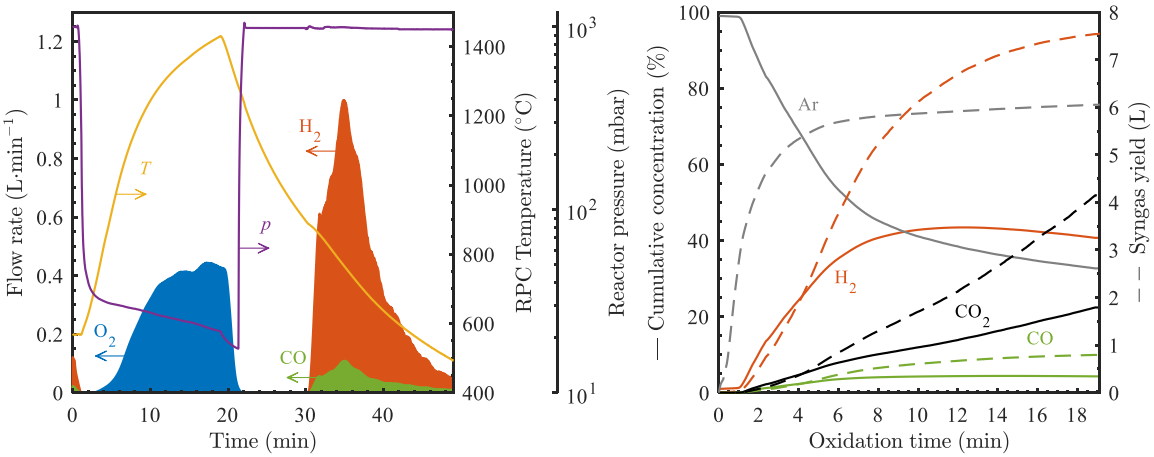


**Figure 9.** Representative solar redox cycle producing syngas with composition suitable for methanol synthesis. a) Temporal variation of the nominal cavity temperature, total pressure, and outlet gas flow rates during a single redox cycle. b) Temporal variation of the cumulative species concentration and yield of solar syngas collected during the oxidation step. Operation conditions – During the reduction step: $Q_{solar}$ = 5.1 kW, inlet flow 0.5 L/min Ar, $T_{reduction\text{-}end}$ = 1450°C, total pressure ≤ 25 mbar. During the oxidation step: $Q_{solar}$ = 0 kW, inlet flows 0.4 L/min $CO_2$ + 9.8 g/min $H_2O$, $T_{oxidation\text{-}start}$ = 900°C, total pressure = 1 bar.

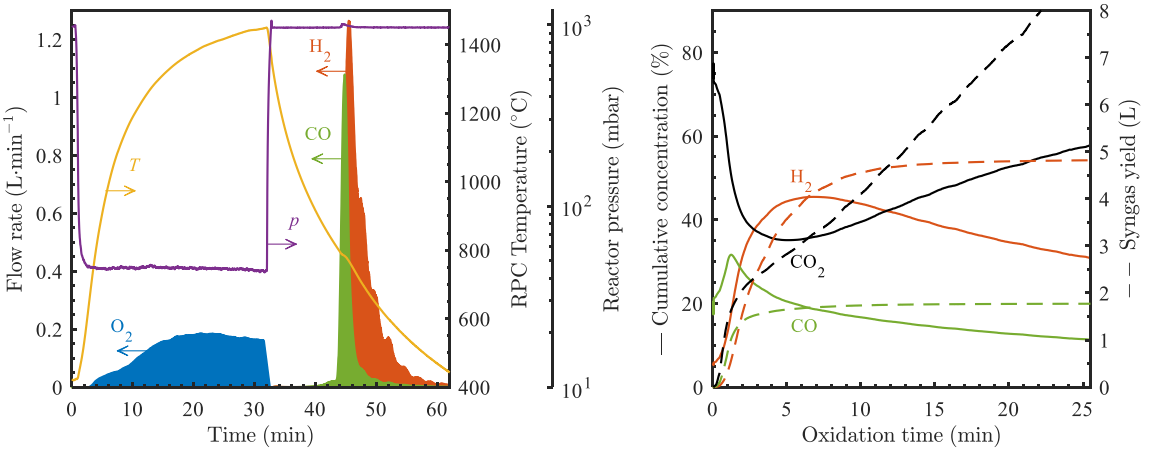


**Figure 10.** Representative solar redox cycle producing syngas with composition suitable for FT synthesis. a) Temporal variation of the nominal cavity temperature, total pressure, and outlet gas flow rates during a single redox cycle. b) Temporal variation of the cumulative species concentration and yield of solar syngas collected during the oxidation step. Operation conditions – During the reduction step: $Q_{solar}$ = 4.1 kW, inlet flow 0.5 L/min Ar, $T_{reduction\text{-}end}$ = 1450°C, total pressure ≤ 50 mbar. During the oxidation step: $Q_{solar}$ = 0 kW, inlet flows 0.2 L/min $CO_2$ + 9.8 g/min $H_2O$, $T_{oxidation\text{-}start}$ = 800°C, total pressure = 1 bar.

### 4.4 Mass balance

In both redox cycles for Figs. 9 and 10, the oxygen mass balance can be closed within the error bars of the measurement devices (electronic mass flow controllers and the electrochemical and IR gas analysis), confirming total selectivity for the conversion of $H_2O$ to $H_2$ and of $CO_2$ to CO, with net reactions $H_2O = H_2 + ½O_2$ and $CO_2 = CO + ½O_2$. Total selectivity was obtained in all cycles performed with the solar reactor.

### 4.5 Long-term consecutive solar redox cycling for methanol production

Figure 11a shows the syngas composition and yield for each of the 152 consecutive solar redox cycles. The reactants' flow rates during the oxidation step were 0.4 L/min $CO_2$ and 10 g/min $H_2O$ for cycles 1 to 37, and 0.3 L/min $CO_2$ and 10 g/min $H_2O$ for cycles 38 to 152. During the first 17 cycles, a molar ratio $H_2$:$CO_x$ = 2 was targeted. From cycle 18 onwards, a cumulative molar ratio $H_2$:$CO_x$ = 2.5 over the entire 152 cycles was targeted. Figure 11b shows the cyclic variation and cumulative molar ratio $H_2$:$CO_x$ for the 152 redox cycles. The total yield was 1069.7 L of syngas with composition 58.4% $H_2$, 5% CO, 18.6% $CO_2$ and 18% Ar (after condensation of unreacted water). Thus, the cumulative molar ratio obtained $H_2$:$CO_x$ = 2.48. This solar syngas was further processed to methanol in the GTL unit.

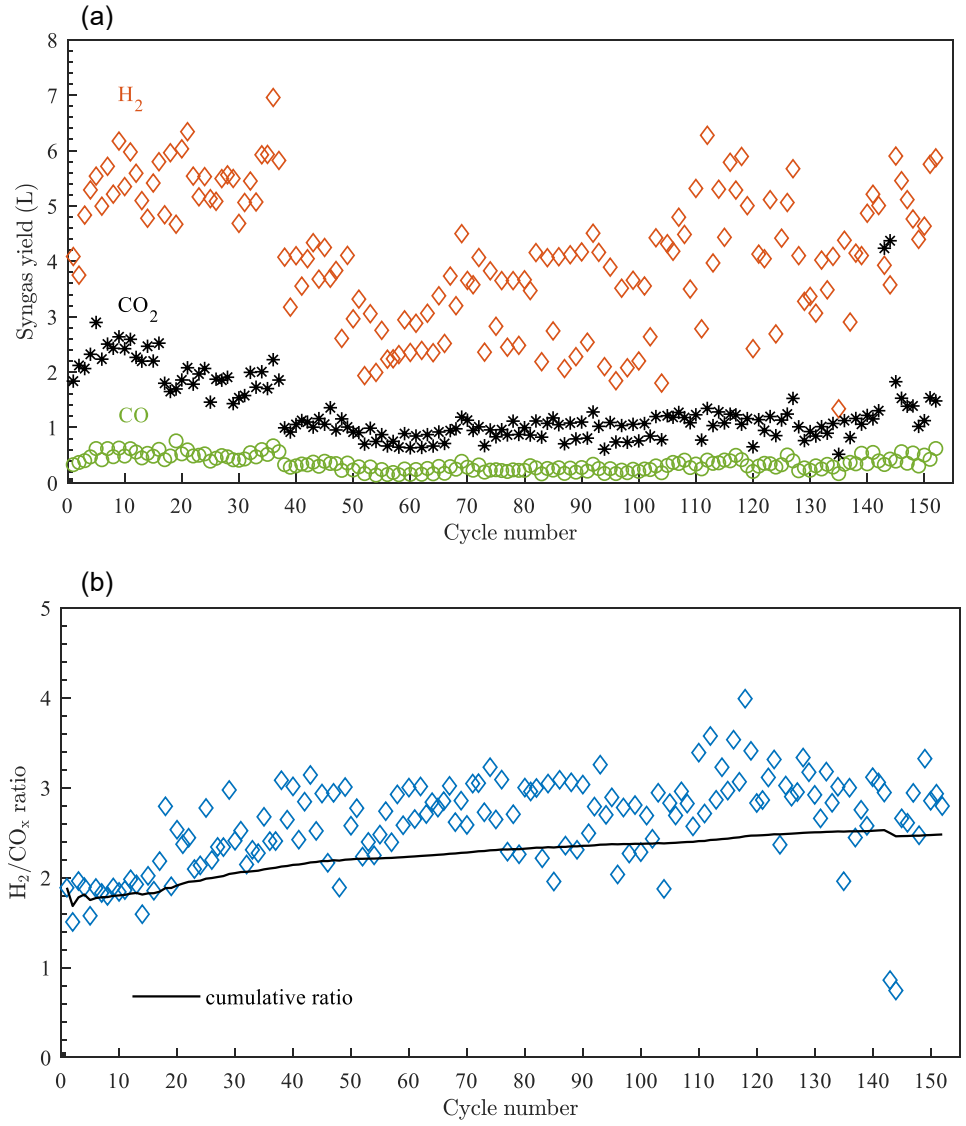


**Figure 11**. a) Syngas yield ($H_2$ in orange, CO in green, $CO_2$ in black) for each of the 152 consecutive solar redox cycles. L denotes standard liters. b) Cyclic variation (blue data points) and cumulative (black curve) molar ratio $H_2$:$CO_x$ for the 152 consecutive redox.

### 4.6 Integration of the solar fuel system

The $CO_2$ and water streams exiting the DAC unit are intermediately stored in a 750 l steel buffer tank and in a plastic buffer tank, respectively. If the $CO_2$ tank reaches 12 bars, usually after 48 hours operation, the DAC unit is automatically idled until demand is present. With this arrangement, both $CO_2$ and $H_2O$ are delivered from their buffer tanks to the solar redox unit on demand. The full $CO_2$ buffer tank can typically support between 3 to 18 days of operation of the solar redox unit, depending on the specific fuel targeted, e.g. 3 to 5 days for $CO_2$ splitting only. Note the mismatch between the amount of water obtained in the DAC unit ($H_2O$:$CO_2$ ~ 6.1-12.2, depending on the air relative humidity) and that used in the solar redox unit ($H_2O$:$CO_2$ ~ 12.5-24.9, depending on the targeted fuel), but the intermediate buffer tanks take care of this mismatch and excess unreacted water collected downstream of the solar reactor can be recycled. The molar ratios $H_2O$:$CO_2$ of reactants fed to the solar redox unit were significantly higher than the stoichiometric ones (Table 1), pointing out to the excess water fed into the solar reactor. This is attributed to the dissociation of $CO_2$ being more thermodynamically favorable than that of $H_2O$ at equal conditions[11]. Excess water introduces significant energy penalties associated with steam generation and heating unreacted species, although a portion of the sensible heat can be recovered. The syngas stream produced by the solar redox unit is intermediately stored in a 5-liter buffer gas cylinder at up to 250 bar before its delivery to the GTL unit. In principle, the GTL unit can be operated continuously round-the-clock by making use of the intermediate buffer storage tank. Alternatively, intermittent daily startup-shutdown operation of the GTL unit for methanol synthesis is technically feasible provided the catalyst is purged with $H_2$-free gas upon shutdown to avoid its deactivation[12]. This option avoids the cost of storing syngas but at the expense of the added complication of operating intermittently an oversized GTL unit.

### 4.7 Energy Efficiency

An important indicator of the economic feasibility of the solar fuel system is its overall energy efficiency $\eta_{\text{system}}$ – defined as the ratio of the heating value of the liquid fuel produced to the total energy input to the system –, which in turn results from multiplying the energy efficiencies of each of the three units. In the present demonstration, we undertook no attempt to optimize the units for maximum $\eta_{\text{system}}$. With thermal management, the DAC unit can be driven by waste heat at below 100°C, available for example from the solar redox unit, while the GTL unit can be operated auto-thermally, thus minimizing the energy penalties upstream and downstream of the solar redox unit. However, the energy efficiency of the solar redox unit dominates $\eta_{\text{system}}$. It results from multiplying the solar optical efficiency $\eta_{\text{optical}}$ – defined as the ratio of the solar radiative energy input to the solar reactor $Q_{\text{solar}}$ to the DNI incident on the solar primary concentrator – and the solar-to-syngas energy efficiency $\eta_{\text{solar-to-syngas}}$ – defined as the ratio of the heating value of the syngas produced to the sum of $Q_{\text{solar}}$ and any other parasitic energy inputs such as the required energy associated with vacuum pumping and/or inert gas consumption during the reduction step.

The solar-to-syngas energy efficiency $\eta_{\text{solar-to-syngas}}$ is defined as:

$$\eta_{\text{solar-to-syngas}} = \frac{Q_{\text{fuel}}}{Q_{\text{input}}} = \frac{Q_{\text{fuel}}}{Q_{\text{solar}} + Q_{\text{pump}} + Q_{\text{inert}}} \tag{3}$$

$Q_{\text{fuel}}$ is the energy content of the fuel (CO and $H_2$) produced over a cycle, given by:

$$Q_{\text{fuel}} = \sum_{\text{fuel: } H_2, CO} \Delta H_{\text{fuel}} \int r_{\text{fuel}} dt \tag{4}$$

where $\Delta H_{\text{fuel}}$ is the molar heating value of the fuel ($\Delta H_{\text{CO}}$=283 kJ/mol, $\Delta H_{\text{H}_2}$ = 286 kJ/mol ) and $\int r_{\text{fuel}} dt$ is the measured molar rate of the fuel produced integrated over the duration of the oxidation step. $Q_{\text{solar}}$ is the total solar energy input integrated over the duration of the reduction step:

$$Q_{\text{solar}} = \int P_{\text{solar}} dt \tag{5}$$

where $P_{\text{solar}}$ is the measured solar radiative power input through the solar reactor's aperture, accounting for the measured 0.932 total transmittance of the quartz window[5]. $Q_{\text{pump}}$ and $Q_{\text{inert}}$ are the thermal energy penalties associated with vacuum pumping and inert gas consumption during the reduction step. Note that all work terms are converted to an equivalent heat by diving by a heat-to-work efficiency $\eta_{\text{heat-to-work}}$ (assumed 0.4). In this way, the entire thermochemical process chain is driven using solar heat alone. $Q_{\text{pump}}$ is calculated as the thermodynamic minimum pumping work divided by the product of two efficiencies, namely the heat-to-work efficiency $\eta_{\text{heat-to-work}}$ and the vacuum pump efficiency $\eta_{\text{pump}}$, according to:

$$Q_{\text{pump}} = \frac{1}{\eta_{\text{heat-to-work}} \cdot \eta_{\text{pump}}} \int \dot{n} \cdot \ln\left(\frac{p_{\text{atmospheric}}}{p_{\text{reactor}}(t)}\right) dt \tag{6}$$

where $\dot{n}$(t) is the sum of the measured molar flow rates of Ar injected and $O_2$ released by ceria during the reduction step. The pump efficiency for a multi-stage industrial arrangement is given by:

$$\eta_{\text{pump}} = 0.07 \cdot \log\left(\frac{p_{\text{total}}}{p_{\text{atmospheric}}}\right) + 0.4 \tag{7}$$

where $p_{\text{total}}$ is the measured total pressure inside the cavity. Note that $\eta_{\text{solar-to-syngas}}$ is weakly depended on $\eta_{\text{pump}}$ because $Q_{\text{solar}}$ >> $Q_{\text{pump}}$ at the moderate vacuum pressure levels applied during reduction in the range 10-1000 mbar. The thermal energy required for inert gas separation is given by:

$$Q_{\text{inert}} = \frac{1}{\eta_{\text{heat-to-work}}} E_{\text{inert}} \int r_{\text{inert}} dt \tag{8}$$

where $r_{\text{inert}}$ is the measured Ar flow rate during reduction and $E_{\text{inert}}$ is the work required for inert gas separation, assumed 20 kJ per mol.. The use of Ar does not affect the chemical reactions but introduces an energy penalty $Q_{\text{inert}}$ of less than 1% of $Q_{\text{solar}}$ because of its low mass flow rate (0.5 L $\text{min}^{-1}$), but even this penalty can in principle be eliminated by replacing Ar with ambient air as proved experimentally.

Based on the measured performance of the present solar redox unit, $\eta_{\text{optical}}$ = 59.6%[30] and $\eta_{\text{solar-to-syngas}}$ = 1.9 – 3.8%. By minimizing surface and tracking errors, $\eta_{\text{optical}}$ can be increased to 82%[30]. Notably, the optical components for concentrating DNI, e.g. solar dishes and heliostat fields, are already established for commercial concentrated solar power (CSP) plants, though for lower values of solar concentration, but there are substantial technological spillovers from solar thermal electricity to solar thermochemical fuels. On the other hand, the low value obtained for $\eta_{\text{solar-to-syngas}}$ is mainly due to the sensible heat rejected during the temperature-swing cycling, which accounted for more than 60% of

$Q_{solar}$. This fraction can be partially recovered via thermocline heat storage, as recently demonstrated with a packed bed of $Al_2O_3$ spheres[38]. Recovering only half of it would boost $\eta_{solar\text{-}to\text{-}syngas}$ to over 20%[39,40]. Thus, by means of optimized porous structures, improved concentrating optics, heat recovery, and thermal management to enable thermo-neutral operation of the DAC and GTL units, $\eta_{system}$ has the potential of exceeding 15% and possibly surpassing that of the PV-electrolysis based pathway[15,41,42]. This is because the later requires the production of substantial excess $H_2$ by water electrolysis using solar electricity, which is subsequently consumed via the endothermic RWGS reaction to obtain syngas suitable for the GTL step. In contrast, the present thermochemical approach bypasses the solar electricity generation, the electrolysis, and the RWGS steps, and directly produces solar syngas of desired composition, i.e. three steps are replaced by one.

To date, the maximum experimentally obtained $\eta_{solar\text{-}to\text{-}syngas}$ was 5.25% with a 4-kW solar reactor[27] and 5.6% with a 50-kW solar reactor[34], both solar reactors performing the $CO_2$ splitting redox cycle without any heat recovery.

*Error estimation* – The error in the determination of $\eta_{solar\text{-}to\text{-}syngas}$ (based on the measured performance of the solar reactor) is estimated as +0.8/-0.6. This estimation is derived from a conservative maximum error analysis using the individual measurement uncertainties. The uncertainty of $Q_{solar}$ is comprised of the measurement accuracy of the water calorimeter, the accuracy of the pyrheliometer (sensor ±1%; data acquisition ±0.1% of reading, ±0.04% of range) and an error for the alignment of the optical system with the solar reactors (conservative error estimation ±10%). The measurement accuracy of the calorimeter is estimated at ±5% using uncertainty propagation and depends on the solar power (e.g. ±4.8% at 5 kW solar power input). The accuracy of the calorimeter measurement instrumentation includes the liquid mass flow meter (meter ±1.25% of reading, ±0.3% of full scale value, data acquisition ±0.1 mA, corresponding to ±0.1875 L/min) and the RTD temperature measurements (sensor energy ±0.15 + (0.002 · T) °C, data acquisition ±0.15 °C). The uncertainties of $Q_{fuel}$ and $Q_{inert}$ are based on the accuracies of the mass flow meters (sensor ±0.5% of reading, ±0.1% of full scale value; gas conversion factor ±2% of conversion factor; data acquisition ±0.04% of reading, ±0.07% of range) and gas analysis units (sensor ±2% of full scale value, ±1% of measuring range, signal noise ±1% of measuring range; data acquisition ±0.87% of reading, ±0.05% of range). The uncertainties of $Q_{pump}$ include the accuracy of the pressure sensors (sensor ±0.75% of reading; data acquisition ±0.52% of reading, ±0.04% of range).

*System energy efficiency* – The system (overall) energy efficiency $\eta_{system}$ is defined as the ratio of the heating value of the liquid fuel produced to the total energy input to the system, which in turn results from multiplying the energy efficiencies of each of the three units of the process chain:

$$\eta_{system} = \eta_{DAC} \cdot \eta_{solar\ redox\ unit} \cdot \eta_{GTL} \tag{9}$$

With thermal management, the thermal energy requirements of the DAC unit can be provided by waste heat available from the solar redox unit. Since the equivalent thermal energy penalty for vacuum pumping 1 mol of $CO_2$ (13 kJ / $\eta_{heat\text{-}to\text{-}work}$) represents about 5% of the molar heating value of methanol (638 kJ/mol), $\eta_{DAC} \approx 0.95$. With improved optics ($\eta_{optical} > 0.8$ [30]), optimized redox structure, and heat recovery (> 50% using thermocline-based heat storage), $\eta_{solar\text{-}to\text{-}syngas} > 0.2$. The GTL unit can be

operated auto-thermally ($\Delta H$ = -90 kJ/mol $CH_3OH$). Assuming 90% mass conversion[44], $\eta_{GTL} \approx 0.79$. Thus, $\eta_{system}$ has the potential of exceeding 15%.

*Economics* – Techno-economic analyses of the complete process chain analogous to the pathway demonstrated in this study[42-44] estimated a jet fuel cost in the range 1.6 – 2.5 USD per liter. These values are sensitive to the manufacturing costs of the heliostat field, which typically represent half of the total investments costs of the solar fuel system. This also explains the strong dependency of the fuel cost on the solar reactor performance because the higher $\eta_{solar\text{-}to\text{-}syngas}$ the smaller becomes the heliostat field for a given $Q_{solar}$. As expected, solar thermochemical fuels are most competitively produced in desert regions with high DNI (> 2500 kWh·m$^{-2}$ per year)[44]. In contrast to biofuels, which are limited by resource provision, global jet fuel demand can be met by utilizing less than 1% of the worldwide arid land[43], which does not compete with food or fodder production. Furthermore, the solar fuel production chain's life cycle assessment indicates savings of 80% with respect to conventional jet fuel, with greenhouse gas emissions in the range 0.1-0.6 $kg_{CO2\text{-}equivalent}$ per liter jet fuel and approaching zero when construction materials (e.g. steel, glass) are manufactured using renewable energy[44], as the amount of $CO_2$ emitted during combustion equals that captured from the air during its production.

# 5 Conclusions

The entire thermochemical process chain to liquid hydrocarbon fuels from sunlight and air was demonstrated for the first time in a solar mini-refinery system mounted on the roof of the ETH-Machine Laboratory. Using concentrated solar radiation, a high-temperature solar reactor splits $CO_2$ and $H_2O$ extracted directly from ambient air and produces syngas – a specific mixture of $H_2$ and CO – which is finally processed into liquid hydrocarbons such as methanol or kerosene. The stable experimental results of the complete integrated system obtained under real field conditions and intermittent solar irradiation provide compelling evidence of the technical viability of the thermochemical process chain for converting sunlight and ambient air to drop-in fuels.

# 6 Outlook and next steps

The next actions to bring these solar fuels to the market include technological improvements and upscaling, and implementation of appropriate policy schemes to enable market introduction at commercial scale.

*Scaling up* – A 10x scale of the solar reactor has already been tested in a solar tower[34,35]. There is room for optimization of the ceria structure, for example by means of 3D-printed hierarchically ordered structures with a porosity gradient for improved volumetric absorption[37]. Since the size of the front quartz window is limited, the commercial-size MW solar tower plant foresees an array of solar reactor modules, each attached to hexagon-shaped secondary concentrators in a honeycomb arrangement. Further assembling the array of solar reactor modules in at least two clusters and focusing the heliostat field alternately onto each cluster would enable the continuous operation of both redox steps of the cycle. This re-focusing of the heliostat field should be feasible with current hardware/software control but its dynamics still needs to be proven in the field.

*Policy to bring solar fuels to market* – Regulatory frameworks progress over time to match three phases: initial R&D and technology demonstration, market creation and system development, and market competitiveness[45-47]. The immediate challenge for solar fuels is to move them from the first to the second phase. However, existing policies such as CORSIA or the EU Emission Trading System are unsuited because they do not create market demand for solar fuels, as their carbon-pricing support is too low to push current solar fuels into the market. To create a near-term market for the first generation of commercial solar fuel plants and start the trip down the learning curve, we propose an aviation sector support scheme: a jet fuel quota scheme, mandating aviation fuel retailers or airlines to provide certificates proving that a certain proportion of the fuel comes from solar fuel sources. The initial costs of such a policy would be small enough to be politically feasible, because the initial quota would be very low relative to overall jet fuel demand. For example, a plant with ten commercial solar towers, each for 100 $MW_{thermal}$ with $\eta_{system}$ = 10%, could produce roughly 30 million liters of jet fuel annually, corresponding to less than 0.01% of global jet fuel consumption. Even if the initial cost were to exceed 10 USD per liter jet fuel, the financial impact of supplying 0.01% of the market would be negligible. Nevertheless, it would trigger deployment of production facilities, which is the main aim of the policy. Importantly, solar drop-in fuels can continue to use the existing massive infrastructures for fuel storage, distribution, and utilization. Thus, unlike other sectors being decarbonized, solar drop-in fuels do not require new market designs, no new distribution networks, and no new technologies beyond the production chain. In sum, the demonstration of the entire production chain from sunlight and air to carbon-neutral hydrocarbon fuels represents a technological milestone with potentially large policy implications for the complete decarbonization of the aviation sector.

# 7 National and international cooperation

**University of Zurich**
Institute of Inorganic Chemistry
Winterthurerstrasse 190, Switzerland
Prof. Dr. Greta R. Patzke

**EU-Project SUN-to-LIQUID**
**Bauhaus Luftfahrt**
Lyonel-Reininger-Str. 28, D-80807 Munich, Germany
Dr. Andreas Sitzmann

**German Aerospace Center**
Institute of Solar Research
Lindner Höhe, D-51147 Köln, Germany
Prof. Dr. Robert Pitz-Paal
**IMDEA-Energy**
Avda. Ramon de la Sagra 3, Madrid, Spain
Dr. Manuel Romero

# 8 Communication

- 1 press release and 4 internal articles by ETH
- 12 TV reports, including SRF1 “Tagesschau” and “10vor10”
- 5 radio reports and interviews
- 23 print articles in newspapers and magazines
- 107 on-line reports in newspaper and magazines
- See complete list and direct links at: https://prec.ethz.ch/about-us/news-events/news-archive/fuels-sunlight-air-press-coverage.html

**Selected TV reports**:

| | | |
|---|---|---|
| SRF 1, 10 vor 10 | ETH-Forschern ist es gelungen, Benzin aus Luft und Sonnenlicht herzustellen<br>https://www.srf.ch/play/tv/10vor10/video/treibstoff-aus-luft-und-sonnenlicht?urn=urn:srf:video:f87c2ea2-d9f9-40fd-a286-ae3f2e1359fb | 13.6.2019 |
| SRF 1, Tagesschau Hauptausgabe | Umweltfreundlicher Treibstoff – aus Sonnenlicht und Luft<br>https://www.srf.ch/play/tv/tagesschau/video/umweltfreundlicher-treibstoff---aus-sonnenlicht-und-luft?urn=urn:srf:video:7aa6c95e-212a-45fb-954e-a45c90539704 | 13.06.2019 |
| RTS Un, Le journal 19h30 | EPFZ: mini-raffinerie solaire pour du carburant neutre en carbone<br>https://avenue.argusdatainsights.ch/kundenartikel_archiv/2019-06/1086740/73827383.pdf | 13.06.2019 |
| RSI LA 1, Telegiornale sera | Carburanti ecologici in arrivo<br>https://avenue.argusdatainsights.ch/kundenartikel_archiv/2019-06/1086740/73827519.pdf | 13.06.2019 |
| Tele Züri \| Züriinfo | ETH entwickelt Flugzeugtreibstoff aus Luft und Sonnenlicht<br>https://www.telezueri.ch/zueriinfo/eth-entwickelt-flugzeugtreibstoff-aus-luft-und-sonnenlicht-134611221 | 13.06.2019 |
| nau.ch | ETH: Aus Luft und Licht soll Treibstoff entstehen<br>https://media.nau.ch/videos/lEwxq5KX9vkoV1GgOYyqJbYQd3Rjz4rpPWeBmbZJ/video.mp4 | 15.06.2019 |
| BBC 4tech | Fuels from sunlightand air (in Arabic)<br>https://www.youtube.com/watch?v=VmdRc2_mnAc&feature=youtu.be | 17.09.2019 |
| SRF1 EINSTEIN | Die Jäger der ultimativen Energiequelle (MP4, 75.4 MB)<br>https://ethz.ch/content/dam/ethz/special-interest/mavt/energy-technology/renewable-energy-carriers-dam/media/EINSTEIN%202-1-2020.mp4 | 02.01.2020 |
| SRF1 Nano | Treibstoff aus Sonne, Luft und Wasser<br>https://avenue.argusdatainsights.ch/Article/AvenueClip?artikelHash=1a678dd7a510430aa70df2e4bec5f777_537083E5C6EF4CA1BC75872BA394FE07&artikelDateiId=247741266 | 07.04.2020 |

- Special event: “Inauguration of the Solar Mini-Refinery”, ETH Zurich, 19-6-2019.


# 9 Publications

## 9.1 Papers in refereed journals


1. Furler P., Steinfeld A., "Heat transfer and fluid flow analysis of a 4 kW solar thermochemical reactor for ceria redox cycling", *Chemical Engineering Science*, Vol. 137, pp. 373-383, 2015.
2. Dähler F., Ambrosetti G., Montoya-Zegarra J., Schindler K., Steinfeld A., "High-concentration solar dishes based on pneumatic reflecting membranes", *Solar Energy*, Vol. 124, pp. 89-100, 2016.
3. Ash-Kurlander U., Martin O., Fontana L., Patil V., Bernegger M., Mondelli C., Pérez-Ramírez J., Steinfeld A., "Impact of Daily Startup-Shutdown Conditions on the Production of Solar Methanol over a Commercial Cu-ZnO-Al2O3 Catalyst", *Energy Technology*, Vol. 4, pp. 565-572, 2016.
4. Takacs M., Ackermann S., Bonk A., Neises-von Puttkamer M., Haueter P., Scheffe J.R.. Vogt U.F., Steinfeld A., "Splitting $CO_2$ with a ceria-based redox cycle in a solar-driven thermogravimetric analyzer", *AIChE Journal*, Vol. 63, pp. 1263-1271, 2017.
5. Ackermann S., Steinfeld A., "Spectral hemispherical reflectivity of nonstoichiometric cerium dioxide", *Solar Energy Materials and Solar Cells*, Vol. 159, pp. 167–171, 2017.
6. Dähler F., Wild M., Schäppi R., Haueter P., Cooper T., Good P., Larrea C., Schmitz M., Furler P., Steinfeld A., "Optical design and experimental characterization of a solar concentrating dish system for fuel production via thermochemical redox cycles", *Solar Energy*, Vol. 170, pp. 568-575, 2018.
7. Bulfin B., Buttsworth L., Lidor A., Steinfeld A., "High-purity nitrogen production from air by pressure swing adsorption combined with SrFeO3 redox chemical looping", *Chemical Engineering Journal*, Vol. 421, pp. 127734, 2021.
8. Madhusudhan J, Ritter C., Bulfin B., Steinfeld A., Erni R., Patzke G., "Reversible phase transformations in novel Ce-substituted perovskite oxide composites for solar thermochemical redox splitting of $CO_2$", *Advanced Energy Materials*, Vol. 11, 2003532, 2021.
9. Bulfin B., Miranda M., Steinfeld A., "Performance Indicators for Benchmarking Solar Thermochemical Fuel Processes and Reactors", *Frontiers in Energy Research*, Vol. 9, Art. 677980, 2021.
10. **Schäppi R., Rutz D., Dähler F., Muroyama A., Haueter P., Lilliestam J., Patt A., Furler P., Steinfeld A., "Drop-in fuels from sunlight and air", *Nature*, in press 2021, https://www.nature.com/articles/s41586-021-04174-y**


## 9.2 Conference contributions


1. Cooper T., Marxer D., Furler P., Steinfeld A., "Solar thermochemical production of liquid hydrocarbon fuels from $H_2O$ and $CO_2$ via redox cycling", 1$^{st}$ *Solar Fuels Conference*, Uppsala, April 26-May 1, 2015.
2. Marxer D., Furler P., Vogt U., Bonk A., Steinfeld A., "Solar-thermochemical splitting of H2O and CO2 via a ceria redox cycle", *Hypothesis XI*, Toledo, Spain, Sept. 7-9, 2015.
3. Haueter P., Marxer D., Furler P., Steinfeld A., "Liquid transportation fuels via solar thermochemical splitting of $H_2O$ and $CO_2$", *21$^{st}$ Solarpaces Conference*, Cape Town, South Africa, Oct. 13-16, 2015.

4. Furler P., Marxer D., Steinfeld A., "Wie kann man aus $CO_2$, $H_2O$ und Sonnenlicht Kraftstoffe herstellen? *ETH Klimarunde*, Zurich, Switzerland, 4-11-2015.
5. Marxer D., Furler P., Haueter P., Steinfeld A., "A solar vacuum-swing thermochemical reactor for splitting of $H_2O$ and $CO_2$ via ceria redox reactions", *ASME Power & Energy Conference*, Charlotte, USA, June 26-30, 2016.
6. Muhich C., Steinfeld A., "Materials and components for thermochemical syngas generation: Overview of work at ETH", *VI Solar Syngas Workshop*, Technical University Clausthal, Germany, June 1-2, 2016.
7. Furler P., Marxer D., Haueter P., Steinfeld A., "Solar Kerosene from $H_2O$ and $CO_2$", *22nd Solarpaces International Conference*, Abu Dhabi, United Arab Emirates, Oct. 11-14, 2016. AIP Conferemce
8. Muhich C., Hoes M., Steinfeld A., "Advanced redox materials for the solar-driven thermochemical splitting of $H_2O$ and $CO_2$", *Tailor-Made Fuels from Biomass: 5th International Conference*, Aachen, Germany, June 20-22, 2017.
9. Furler P., Marxer D., Takacs M., Steinfeld A., "Solar thermochemical reactor technology for splitting $CO_2$ and $H_2O$", *23rd SOLARPACES Conference*, Santiago, Chile, Sept. 26-29, 2017; *AIP Conference Proceedings* 2033, 130005-1–130005-4, 2018.
10. Schäppi R., Rutz D., Basler P., Muroyama A., Haueter P., Furler P. Steinfeld A. , "Solar Thermochemical Splitting of $CO_2$ in a Modular Solar Dish-Reactor System", *Proc. ISES-SWC2019 Solar World Congress*, Santiago, Chile, Nov. 4-7, 2019. doi:10.18086/swc.2019.24.08
11. Dähler F., Wild M., Schäppi R., Haueter P., Cooper T., Furler P., Steinfeld A., "A High-Flux Solar Parabolic Dish System for Continuous Thermochemical Fuel Production", *OSA Light, Energy and the Environment Congress*, Boulder, USA, Nov. 6-9, 2017.
12. Furler P., Marxer D., Takacs M., Steinfeld A., "Solar thermochemical splitting of CO2 and H2O with high selectivity, stability, conversion, and efficiency", *12th Int. Symposium Hydrogen & Energy*, EPFL, Laussane, Switzerland, Feb. 16, 2018.
13. Muhich C., Hoes M., Blaser S., Steinfeld A., "Examining the solar-to-fuel efficiency of ceria and perovskite thermochemical redox cycles for splitting $H_2O$ and $CO_2$", *AIChE Annual Meeting* - International Congress on Energy, Pittsburgh, USA. Oct. 28 – Nov. 2, 2018.
14. Bulfin B., Koepf E., Furler P., Steinfeld A., "Solar Thermochemical Fuel Processing from $H_2O$ and $CO_2$", *Euroscience Open Forum*, Toulouse, July 12, 2018.
15. Muroyama A., Steinfeld A., "Solar Thermochemical Production of Fuels from $H_2O$ and $CO_2$", *4th Symposium*, Evora, Portugal, Sept. 24-25, 2018.
16. Schäppi R., Rutz D., Dähler F., Haueter P., Furler P, Steinfeld A., "Methanol from Sunlight and Air Using a Modular Solar Dish Reactor System", *2020 AIChE Annual Meeting*, San Francisco, USA, Nov. 15-20, 2020.
17. Schäppi R., Haueter P., Furler P., Steinfeld A., "Solar Fuel Production from Ambient Air in a Modular Solar Concentrator-Reactor System", *2021 ASME Energy Sustainability,* June 16-18, 2021.
18. Schäppi R., Haueter P., Furler P., Steinfeld A., "Solar Syngas Production from $H_2O$ and $CO_2$ applicable for Methanol or Fischer-Tropsch Synthesis", *2021 AIChE Annual Meeting - Sustainable Engineering Forum*, Boston, USA, Nov. 7-12, 2021.

### 9.3 Invited talks

1. Steinfeld A., "Solar thermochemical splitting of $CO_2$ into separate streams of CO and $O_2$ with high selectivity, stability, conversion, and efficiency", *Connaught Global Challenge Symposium*, Toronto, 9.5.2017.
2. Steinfeld A., "Novel materials and processes for concentrated solar power & fuels", Plenary Speaker, *9th World Conference on Experimental Heat Transfer, Fluid Mechanics, and Thermodynamics*, Iguazu, Brazil, 13.6. 2017.
3. Steinfeld A., "Solar jet fuel made out of thin air", Plenary Speaker, *ASME Heat Transfer Conference*, Bellevue, WA, USA, 9-14 July 2017.
4. Steinfeld A., "Jet fuel from $H_2O$, $CO_2$, and solar energy", *Boelter Chair Colloquium,* University of California Los Angeles, Oct. 20, 2017.
5. Steinfeld A., "Jet Fuel from $H_2O$, $CO_2$, and Solar Energy", Keynote, *2017 AIChE Annual Meeting*, Minneapolis, USA, Oct. 31, 2017.
6. Steinfeld A., "Jet Fuel from $H_2O$, $CO_2$, and Solar Energy", *Precourt Institute for Energy,* Stanford University, USA, Nov. 17, 2017.
7. Steinfeld A., "Jet Fuel from $H_2O$, $CO_2$, and Solar Energy", University of Arizona, USA, Nov. 17, 2017.
8. Steinfeld A., "Drop-in Transportation Fuels from $H_2O$, $CO_2$, and Solar Energy", University of Brescia, 25.6.2019.
9. Schäppi R., "CO2-neutrale Treibstoffe aus Luft und Sonnenlicht", *Scientifica – Zürcher Wissenschaftstage*, ETH Zürich, Sept. 1, 2019.
10. Steinfeld A., "Drop-in Fuels from Sunlight and Air", EDEY Doctoral School, EPFL, 11.12.2019.
11. Schäppi R., Dähler F., Haueter P., Furler P. Steinfeld A., "Treibstoff aus Luft und Sonnenlicht", *Treffpunkt Science City*, Nov. 22, 2020.
12. Schäppi R., Dähler F., Haueter P., Furler P. Steinfeld A., "Treibstoff aus Luft und Sonnenlicht", *Richard Vollenweider Lectures*, Kantonsschule Musegg, Luzern, Switzerland, 04.12.2020.
13. Schäppi R., Dähler F., Haueter P., Furler P. Steinfeld A., "Thermochemical fuel production from sunlight and air", *EIT Urban Mobility 2020*, Technion, Israel, Dec. 7-9, 2020.
1. Steinfeld A., "Drop-in Fuels from Sunlight and Air", EDEY Doctoral School, EPFL, 11.12.2019.
2. Steinfeld A., "Transportation Fuels from Sunlight and Air", Distinguished Seminars of the Solar Energy Research Center, Chile, 15.1.2021.
14. Steinfeld A. "Sustainable Transportation Fuels from $H_2O$ and $CO_2$ using Concentrated Solar Energy", *11th SOLARIS Internatioal Symposium on Solar Enegy and Efficient Energy Usage*, Tokyo, 27.9.2021.

# 10 References


1 Grote, M. et al. Direct carbon dioxide emissions from civil aircraft. *Atmospheric Environment* **95**, 214-224 (2014).

2 Eyring, V. et al. Emissions from international shipping: 2. Impact of future technologies on scenarios until 2050. *Journal of Geophysical Research* **110**, D17306 (2005).

3 Mayor, K, & Toll, R. Scenarios of carbon dioxide emissions from aviation, *Global Environmental Change* **20**, 65–73 (2010).

4 Schäfer, A. et al. Technological, economic and environmental prospects of all-electric aircraft. *Nature Energy* **4**, 160–166 (2019).

5 Lewis, N.S., & Nocera, D.G. Powering the planet: chemical challenges in solar energy utilization. *Proc Natl Acad Sci* **103**, 15729-15735 (2006).

6 Ozin, G.A. Throwing new light on the reduction of CO2. *Advanced Materials* **27**, 1957-1963 (2015).

7 Detz, R.J. et al. The future of solar fuels: when could they become competitive?. *Energy & Environmental Science* **11**, 1653-1669 (2018).

8 Romero, M. & Steinfeld, A. Concentrating solar thermal power and thermochemical fuels. *Energy & Environmental Science* **5**, 9234-9245 (2012).

9 Zeman, F. S., & Keith, D. W. Carbon neutral hydrocarbons. *Phil. Trans. R. Soc. A* **366**, 3901-3918 (2008).

10 Wurzbacher, J. et al. Concurrent separation of $CO_2$ and $H_2O$ from air by a temperature-vacuum swing adsorption/desorption cycle. *Environmental Science & Technology* **46**, 9191-9198 (2012).

11 Brady C. et al. Integration of thermochemical water splitting with CO2 direct air capture. *Proceedings of the National Academy of Sciences of the United States of America* **116**, 25001-25007 (2019).

12 Jia, J. et al. Solar water splitting by photovoltaic-electrolysis with a solar-to-hydrogen efficiency over 30%. *Nature Communications* **7,** 13237 (2016).

13 Chalmin A. Direct air capture: recent developments and future plans. *Geoengineering Monitor* (2019).

14 Roeb, M. et al. Test operation of a 100 kW pilot plant for solar hydrogen production from water on a solar tower. *Solar Energy* **85**, 634–644 (2011).

15 Vázquez F. V. et al. Power-to-X technology using renewable electricity and carbon dioxide from ambient air: SOLETAIR proof-of-concept and improved process concept. *Journal of CO2 Utilization* **28**, 235-246 (2018).

16 Chueh, W.C. & Haile, S.M. A thermochemical study of ceria: exploiting an old material for new modes of energy conversion and CO2 mitigation. *Philosophical Transactions of the Royal Society A: Mathematical, Physical and Engineering Sciences* **368**, 3269-3294 (2010).

17 Abanades, S. & Flamant, G. Thermochemical hydrogen production from a two-step solar-driven water-splitting cycle based on cerium oxides. *Solar Energy* **80**, 1611-1623 (2006).

18 Scheffe, J. R. *et al.* Lanthanum-strontium-manganese perovskites as redox materials for solar thermochemical splitting of $H_2O$ and $CO_2$. *Energy Fuels* **27**, 4250–4257 (2013).

19 McDaniel, A. H. *et al.* Sr- and Mn-doped LaAlO3-δ for solar thermochemical H2 and CO production. *Energy & Environmental Science* **6**, 2424-2428 (2013)

20 Dey, S. *et al.* Noteworthy performance of La1-xCaxMnO3 perovskites in generating H2 and CO by the thermochemical splitting of H2O and CO2. *Physical Chemistry Chemical Physics* **17**, 122-125 (2015).

21 Li, S. et al. Thermodynamic Analyses of Fuel Production via Solar-Driven Nonstoichiometric Metal Oxide Redox Cycling. Part 2. Impact of Solid−Gas Flow Configurations and Active Material Composition on System-Level Efficiency. *Energy Fuels* **32**, 10848−10863 (2018).

22 Muhich, C.L. et al. Efficient generation of $H_2$ by splitting water with an isothermal redox cycle. *Science* **341**, 540-542 (2013).

23 Bader, R. et al. Thermodynamic analysis of isothermal redox cycling of ceria for solar fuel production. *Energy Fuels* **27**, 5533-5544 (2013).

24 Ermanoski, I. et al. Efficiency maximization in solar-thermochemical fuel production: challenging the concept of isothermal water splitting. *Physical Chemistry Chemical Physics* **16**, 8418-8427 (2014).

25 Venstrom, L.J. et al. Efficient splitting of $CO_2$ in an isothermal redox cycle based on ceria. *Energy Fuels* 28, 2732−2742 (2014).

26 Chueh, W.C. et al. High-flux solar-driven thermochemical dissociation of $CO_2$ and $H_2O$ using nonstoichiometric ceria. *Science* **330**, 1797-1801 (2010).

27 Marxer, D. et al. Solar thermochemical splitting of $CO_2$ into separate streams of CO and $O_2$ with high selectivity, stability, conversion, and efficiency. *Energy & Environmental Science* **10**, 1142-1149 (2017).

28 Furler, P. & Steinfeld, A. Heat transfer and fluid flow analysis of a 4 kW solar thermochemical reactor for ceria redox cycling. *Chemical Engineering Science* **137**, 373-383 (2015).

29 Furler, P. et al. Thermochemical $CO_2$ splitting via redox cycling of ceria reticulated foam structures with dual-scale porosities. *Physical Chemistry Chemical Physics* **16**, 10503-10511 (2014).

30 Dähler, F. et al. Optical design and experimental characterization of a solar concentrating dish system for fuel production via thermochemical redox cycles. *Solar Energy* **170**, 568-575 (2018).

31 Furler, P. et al. Syngas production by simultaneous splitting of $H_2O$ and $CO_2$ via ceria redox reactions in a high-temperature solar reactor. *Energy & Environmental Science* **5**, 6098-6103 (2012).

32 Schäppi, R., et al. Solar Thermochemical Splitting of CO2 in a Modular Solar Dish-Reactor System. *Proc. ISES-SWC2019 Solar World Congress*, Santiago, Chile, Nov. 4-7, 2019. doi:10.18086/swc.2019.24.08

33 Marxer, D. et al. Demonstration of the entire production chain to renewable kerosene via solar thermochemical splitting of $H_2O$ and $CO_2$. *Energy Fuels* **29**, 3241-3250 (2015).

34 Zoller, S. A 50 kW solar thermochemical reactor for syngas production utilizing porous ceria structures. Diss. ETH No. 26451 (2020).

35 Romero, R. et al. Solar-Driven Thermochemical Production of Sustainable Liquid Fuels from $H_2O$ and $CO_2$ in a Heliostat Field. *Proc. ISES-SWC2019 Solar World Congress*, Santiago, Chile, Nov. 4-7, 2019. doi:10.18086/swc.2019.23.02.

36 Corporan, E. et al. Emissions characteristics of a turbine engine and research combustor burning a Fischer-Tropsch jet fuel. *Energy Fuels* **21**, 2615-2626 (2007).

37 Hoes, M. et al. Additive-manufactured ordered porous structures made of ceria for concentrating solar applications. *Energy Technology* submitted.

38 Geissbühler, L. Thermocline thermal energy storage: advances and applications to CSP, compressed air energy storage, and solar fuels. Diss. ETH No. 24555 (2017).

39 Scheffe, J.R. & Steinfeld, A. Thermodynamic Analysis of Cerium-based Oxides for Solar Thermochemical Fuel Production. *Energy Fuels* **26**, 1928-1936 (2012).

40 Lapp, J. *et al.* Efficiency of two-step solar thermochemical non-stoichiometric redox cycles with heat recovery. *Energy* **37**, 591-600 (2012).

41 Wim, H. & Geerlings, H. Efficient production of solar fuel using existing large scale production technologies. *Environ. Sci. Technol.* **45**, 8609–8610 (2011).

42 Kim, J. et al. Fuel production from $CO_2$ using solar-thermal energy: system level analysis. *Energy & Environmental Science* **5**, 8417-8429 (2012).

43 Falter, C. et al. Geographical Potential of Solar Thermochemical Jet Fuel Production. *Energies* **13**, 802, (2020).

44 Falter, C. et al. An integrated techno-economic, environmental and social assessment of the solar thermochemical fuel pathway. *Sustainable Energy & Fuels*, (2020).

45 Perner, J. & Bothe, D. International aspects of a power-to-X roadmap. *Frontier Economics*, 156 (2018).

46 Patt, A. & Lilliestam, J. The case against carbon prices. *Joule* **2**, 2494-2498 (2018).

47 Rosenbloom, D. et al. Why carbon pricing is not sufficient to mitigate climate change - and how "sustainability transition policy" can help. *Proceedings of the National Academy of Sciences* **117**, 8664-8668 (2020).